IOP Publishing New J. Phys. 25 (2023) 033012 https://doi.org/10.1088/1367-2630/acc16a

New Journal of Physics
The open access journal at the forefront of physics

Deutsche Physikalische Gesellschaft DPG
IOP Institute of Physics

Published in partnership with: Deutsche Physikalische Gesellschaft and the Institute of Physics

OPEN ACCESS

RECEIVED
22 August 2022

REVISED
30 January 2023

ACCEPTED FOR PUBLICATION
3 March 2023

PUBLISHED
16 March 2023

PAPER

Analysis of elastic scattering of ^{6}Li by ^{90}Zr near Coulomb barrier

Kamala Kanta Jena[1,2], **Santosh Kumar Agarwalla**[2] **and Bidhubhusan Sahu**[3,*]

[1] P. G. Department of Physics and Applied Physics, Bhadrak Autonomous College, Bhadrak 756100, India
[2] Department of Applied Physics and Ballistics, Fakir Mohan University, Balasore 756019, India
[3] School of Applied Sciences, KIIT Deemed to be University, Bhubaneswar 751024, India
[*] Author to whom any correspondence should be addressed.

E-mail: bbsahufpy@kiit.ac.in

Keywords: elastic scattering, optical potential, reaction cross section, breakup threshold anomaly

Abstract

We use a phenomenological optical potential constructed in consideration of a versatile potential developed by Joseph N. Ginocchio. The optical potential uses less number of energy-dependent parameters to analyse nuclear scattering data. We study the ratios of elastic to Rutherford differential scattering cross sections of the system ^{6}Li + ^{90}Zr at various energies, namely, 10.19, 11.11, 12.07, 13.95, 15.84, 17.71, 19.60, 23.36, 28.05 and 31.87 MeV in the centre-of-mass system. The study of angular distributions is performed in a wide angular range. Our theoretical calculations explain the experimental results and follow breakup threshold anomaly phenomenon near the Coulomb barrier. We discuss the variation of reflection function $|S_l|$ with 'l' for each contributing partial wave and calculate reaction cross section for the system against the projectile energy 31.87 MeV with permissible error.

1. Introduction

It is an established fact that the real part and imaginary part of an optical potential depend upon incident energy in nuclear elastic scattering. The variation is phenomenal near the Coulomb barrier of the scattering systems. However, the dependence is not the same for heavy and light projectiles. Real part of the potential, in case of tightly bound heavy projectiles, remains almost constant at higher energy of incidence, but increases when the incident energy approaches Coulomb barrier. The real part first increases and then decreases showing the variation as a bump (bell-shape) around the barrier. On the other hand, imaginary part remains nearly constant at higher energies, but shows a sharp fall as the energy approaches the Coulomb barrier. Such variation is referred to as *threshold anomaly* (TA) [1]. The systems ^{12}C + ^{208}Pb [2], ^{14}N + ^{90}Zr [3], ^{14}N + ^{56}Fe [4], ^{16}O + ^{208}Pb [5], ^{24}Mg + ^{35}Cl [6], ^{32}S + ^{40}Ca [7], ^{16}O + ^{60}Ni [8], ^{16}O + ^{94}Zr [9], ^{16}O + ^{116}Sn [9], ^{19}F + ^{208}Pb [10] and many more show TA phenomena at low energies.

The dynamics of elastic scattering involving weakly bound nuclei had received impetus during last two decades. When we consider weakly bound light projectiles, the phenomenon may change. The dynamics of the collision for the scattering systems change and the cross sections are also modified in the elastic channel [11]. Such modification is found in ^{6}Li +^{138}Ba [12], ^{9}Be + ^{209}Bi [13], ^{9}Be + ^{64}Zn [14], ^{6}Li + ^{112}Sn [15], ^{6}Li + ^{51}V [16], ^{9}Be + ^{80}Se [17] and many more cases. The imaginary part in case of a scattering system having weak nuclei may increase at the Coulomb barrier and the real part on the other hand may decrease. This phenomenon is known as *break-up threshold anomaly* (BTA).

The findings of scattering experiments are analysed by different models to explore various nuclear properties. Optical model is an established model to study experimental results. This can be accessible to both the elastic and inelastic phenomena, and to a number of phenomena those are relatively complicated [18]. Woods–Saxon (WS) potential, modified WS potential and Gaussian potential are few examples of phenomenological nuclear-potentials those are associated with the optical model analysis. In this paper we use Ginocchio potential to build an optical potential [19–21] for analysis purpose. The short-ranged Ginocchio potential is an analytically solvable asymmetric potential. The optical potential is so built as to take care of the volume as well as the surface regions. The differential scattering cross-sections of the systems

$^{16}O + {}^{28}Si$ and $^{12}C + {}^{24}Mg$ have been successfully explained [19] over wide ranges of energies by using this potential. Further, the authors have used the potential [22, 23] to analyse experimental results of $^{14}N + {}^{56}Fe$, $^{14}N + {}^{90}Zr$ and $^{58}Ni + {}^{27}Al$ for different energy-ranges. We use the optical potential to explain the experimental data of the heavy-ion collision system $^{6}Li + {}^{90}Zr$ at various energies, namely, 10.19, 11.11, 12.07, 13.95, 15.84, 17.71, 19.60, 23.36 and 28.05 MeV in the centre-of-mass frame. We consider the experiments of two teams. The measurements of the system $^{6}Li + {}^{90}Zr$ were performed by Kumawat *et al* [24] by using TIFR-BARC Pelletron facility, Mumbai, India. Elastic scattering data have been measured for the systems $^{6,7}Li + {}^{90,91}Zr$ at 31.87 MeV by Puigh and Kemper [25] by using the Florida State University Super FN Tandem Van de Graaff. We explain the experimental results of both the teams by using our optical potential.

The motivation for choosing the system $^{6}Li + {}^{90}Zr$ lies behind our successful analysis of the elastic system $^{14}N + {}^{90}Zr$ by using the same optical potential [3, 22], in which we consider a tightly bound heavy projectile ^{14}N for ^{90}Zr target. In this article we have chosen a light projectile ^{6}Li which is weakly bound. Analysis for light and heavy projectiles on the same target will show the versatility of the optical potential we have used.

We organise our paper in different sections as follows. We present the formulation of the optical model based on Ginocchio potential in section 2 and the results with discussions in section 3 which contains the application of the optical potential for the analysis of elastic scattering data of system $^{6}Li + {}^{90}Zr$ at various incident energies, discussion on phenomenon of breakup threshold anomaly near Coulomb barrier, variation of reflection function and determination of reaction cross section magnitude at 31.87 MeV. Finally, we present the summary of analysis and main conclusions in section 4.

2. Theoretical formulation

An effective potential to study nuclear interactions essentially consists of a nuclear potential and a Coulomb potential. It may contain a third term contributed by the centrifugal force. Thus, the effective potential may be given by

$$V_{\rm eff}(r) = V_{\rm N}(r) + V_{\rm C}(r) + V_{\rm CF} \tag{1}$$

where, the terms $V_{\rm N}(r)$, $V_{\rm C}(r)$ and $V_{\rm CF}$ represent nuclear potential, Coulomb potential and centrifugal part respectively.

We have taken a complex nuclear potential given by: $V_{\rm N}(r) = V_{\rm n}(r) + {\rm i}W_{\rm n}(r)$. The real part $V_{\rm n}(r)$ of nuclear potential is obtained by modifying an attractive one dimensional potential expressed by Ginocchio [21]. The parameter λ in Ginocchio potential accounts for the shape of the potential and controls the flatness of barrier. The parameter can take any positive value, i.e. $0 < \lambda < \infty$. When $\lambda = 1$, this potential becomes smooth and serves our purpose of analysis of various systems. The details of variation of the parameters of the used potential are illustrated by Sahu *et al* [26]. The imaginary part is framed by following the structure of real part. The real part is expressed [19, 20] as follows.

$$V_n(r) = \begin{cases} -V_{01}\left[B_0 + \frac{B_1 - B_0}{\cosh^2\rho_1}\right], & \text{if } 0 < r < R_0 \\ -V_{02}\left[\frac{B_2}{\cosh^2\rho_2}\right], & \text{if} r \geqslant R_0 \end{cases}. \tag{2}$$

The parameter ρ_1 and ρ_2 are given by $\rho_1 = (r - R_0)b_1$ and $\rho_2 = (r - R_0)b_2$ respectively, by substituting $V_{\rm B} = V_{01}B_1 = V_{02}B_2$ and $b_n = \frac{\sqrt{2\mu V_{\rm B}}}{\hbar^2 B_n}$ with $n = 1, 2$. The parameter R_0 represents radial distance in the surface region and it is close to the radial position of the effective S-wave barrier potential in equation (1). The parameter B_0 controls the depth of potential at the origin ($r = 0$), and $V_{\rm B}$ indicates the depth of potential at $r = R_0$. The slope parameter b_n is simultaneously controlled by B_n and V_{0n} on either side of the radial distance R_0. A small value of B_n gives a large b_n value which the potential changes sharply for. The real part $V_n(r)$ is shown in figure 1 with a set of suitable parameters.

The imaginary part $W_n(r)$ of our nuclear potential has similar form as that of real part, but weaker in strength. This is expressed by equation (3) with a substitution of $V_{0{\rm n}W} = V_{\rm BW}/W_{\rm n}$.

$$W_n(r) = \begin{cases} -V_{01W}\left[W_0 + \frac{W_1 - W_0}{\cosh^2\rho 1}\right], & \text{if } 0 < r < \text{Row} \\ -V_{02W}\left[\frac{W_2}{\cosh^2\rho 2}\right], & \text{if } r \geqslant \text{Row} \end{cases}. \tag{3}$$

The imaginary part of the nuclear potential is plotted in figure 2 against 'r' with a set of suitable parameters as mentioned in its caption.

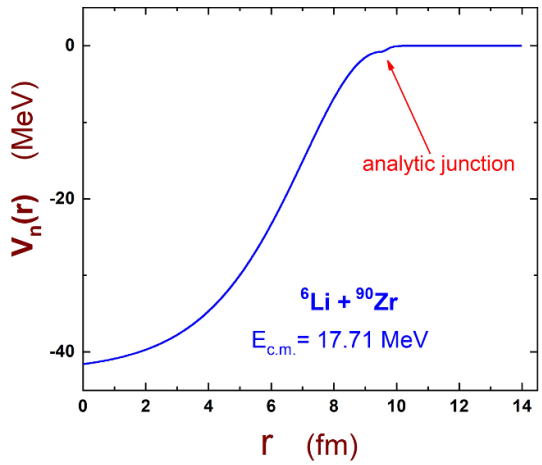

Figure 1. Real part $V_n(r)$ of the nuclear potential for the system ^{6}Li + ^{90}Zr as described in equation (2). The parameters are $R_0 = 9.9$ fm, $V_B = 0.9$ MeV, $B_0 = 42.6$ MeV, $B_1 = 3.0$ and $B_2 = 0.15$ at incident energy $E_{c.m.} = 17.71$ MeV.

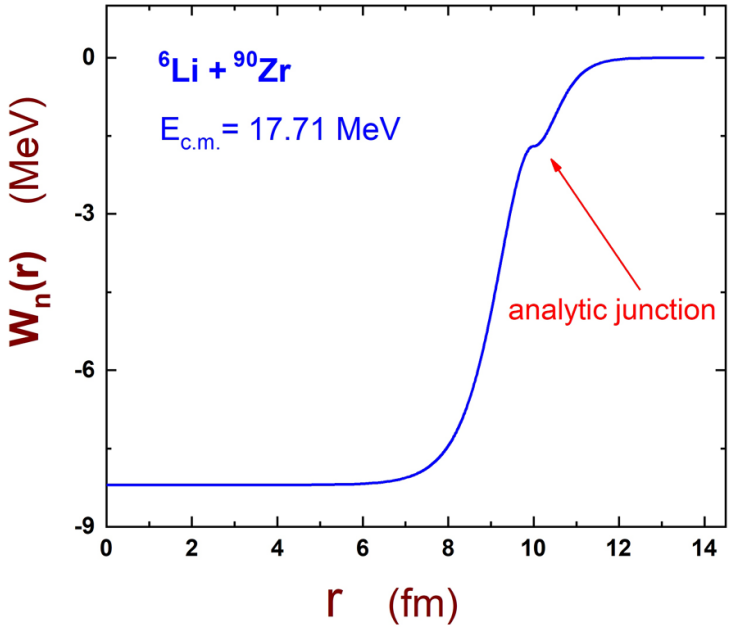

Figure 2. Imaginary part $W_n(r)$ of the nuclear potential for the elastic system ^{6}Li + ^{90}Zr as described in equation (3). The parameters of $W_n(r)$ are $R_{0W} = 10.5$ fm, $V_{BW} = 1.7$ MeV, $W_0 = 8.2$ MeV, $W_1 = 0.6$ and $W_2 = 0.09$ at the incident energy $E_{c.m.} = 17.71$ MeV.

If we reduce a two-body problem to one-body problem, then projectile (P) and the target (T) nuclei will behave as a uniformly charged sphere with a reduced radius $R_C = r_C\,(A_P{}^{1/3} + A_T{}^{1/3})$, where, A_P and A_T are the mass numbers of projectile and target nucleus respectively. The parameter r_C is known as Coulomb radius parameter. We have taken the value of r_C to be 1.25 fm in our formulation. With atomic numbers Z_P and Z_T of the projectile and target nucleus respectively, along with the reduced radius R_C of the scattering system, the Coulomb potential $V_C(r)$ between the two colliding nuclei is represented by equation (4) as

$$V_C(r) = \begin{cases} \frac{Z_P Z_T e^2}{2R_C{}^3}\left(3R_C{}^2 - r^2\right), & \text{if } r < R_C \\ \frac{Z_P Z_T e^2}{r}, & \text{if } r > R_C \end{cases}. \tag{4}$$

The third term V_{CF} in equation (1) arises due to centrifugal force. This potential is given by

$$V_{CF} = \frac{l(l+1)\hbar^2}{2\mu r^2}. \tag{5}$$

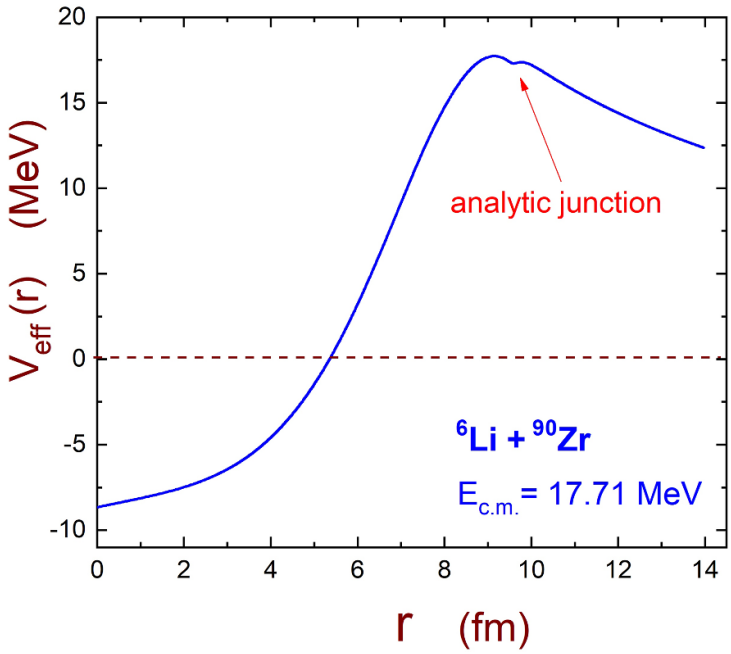

Figure 3. Plot of the effective optical potential $V_{\rm eff}(r)$ for the system ^{6}Li + ^{90}Zr for $l = 0$ at energy $E_{\rm c.m.} = 17.71$ MeV with parameters $R_0 = 9.9$ fm, $V_{\rm B} = 0.9$ MeV, $B_0 = 42.6$ MeV, $B_1 = 3.0$ and $B_2 = 0.15$, $R_{0\rm W} = 10.5$ fm, $V_{\rm BW} = 1.7$ MeV, $W_0 = 8.2$ MeV, $W_1 = 0.6$ and $W_2 = 0.09$ at the incident energy $E_{\rm c.m.} = 17.71$ MeV.

Here, μ is the reduced mass of projectile-target combination which is given by $\mu = \frac{m_1 m_2}{m_1 + m_2}$, where m_1 is the mass of projectile and m_2 is the mass of target. The other parameter 'l' in this term denotes partial wave for a nucleus–nucleus scattering system. The term $V_{\rm CF}$ vanishes for zero value of 'l'.

Our nuclear potential consists of two regions, namely, inner (volume) region and outer (surface) region. Both the regions are analytically solvable, and have different roles to play. They are smoothly joined near $r = R_0$. We refer it to an *analytic junction*, because the junction is analytically solvable and the Schrodinger equation can be solved here. The junction possesses no sudden jerk; rather both the regions coincide here smoothly. Our nuclear potential $V_{\rm N}(r)$ does not decrease monotonically with 'r' unlike the case of standard WS form. The analytic junction feature is clearly shown in the real, imaginary and effective potential curves, which successfully explain the experimental data of differential scattering cross-sections over a wide range of energies in case of ^{6}Li + ^{90}Zr system.

We have taken $l = 0$ in equation (5) to omit the third term in equation (1). The effective potential accepts the form:

$$V_{\rm eff}(r) = V_{\rm N}(r) + V_{\rm C}(r). \tag{6}$$

The effective potential for zero l-value is plotted in the figure 3.

The Schrodinger equation is solved for the effective potential $V_{\rm eff}(r)$ described in equation (1) for the partial waves of different l-values. Total scattering amplitude $f(\theta)$ obtained from the solution of the equation is expressed as the sum of nuclear scattering amplitude $f_{\rm N}(\theta)$ and Coulomb scattering amplitude $f_{\rm C}(\theta)$. Thus,

$$f(\theta) = f_{\rm C}(\theta) + f_{\rm N}(\theta) \tag{7}$$

where,

$$f_{\rm C}(\theta) = \frac{1}{2ik}\sum_{l=0}^{\infty}(2l+1)\left(e^{2i\sigma_l} - 1\right)P_l(cos\theta) \tag{8}$$

$$f_N(\theta) = \frac{1}{2ik}\sum_{l}(2l+1)\,e^{2i\sigma_l}P_l(\cos\theta)\left(e^{2i\bar{\delta}_l} - 1\right). \tag{9}$$

The '*Coulomb*' phase shift due to scattering is denoted by σ_l and the '*nuclear*' phase shift is represented by $\bar{\delta}_l$. We can relate the '*nuclear*' phase shift to '*Coulomb*' phase shift by:

$$\bar{\delta}_l = \delta_l - \sigma_l. \tag{10}$$

The differential cross section of elastic scattering with respect to Rutherford cross-section ($\sigma_{\rm Ruth}$) is given by

$$\frac{d\sigma}{d\sigma_{\rm Ruth}} = \left|\frac{f(\theta)}{f_C(\theta)}\right|^2. \tag{11}$$

For the orbital angular momentum l, the elastic scattering cross section σ_{el} for l^{th} partial wave with the S-matrix S_l may be expressed as

$$\sigma_{\rm el} = \frac{\pi}{k^2}(2l+1)|1-S_l|^2. \tag{12}$$

The elastic scattering results for the system ^{6}Li + ^{90}Zr are discussed below with the above theoretical formalism and optical potential.

3. Results and discussions

3.1. Analysis of scattering cross-sections

We apply the theoretical formulation to analyse experimental data of the heavy ion collision system ^{6}Li + ^{90}Zr. Theoretical ratios of elastic scattering cross-sections ($\sigma_{\rm el}$) to Rutherford scattering cross-sections ($\sigma_{\rm Ruth}$) in a wide angular range in centre of mass frame are compared with the measured angular cross section of elastic scattering for the system considered. The analysis is performed at ten energies of incidence, namely, 10.19, 11.11, 12.07, 13.95, 15.84, 17.71, 19.60, 23.36, 28.05 and 31.87 MeV in the centre-of-mass frame. We use ten parameters in the optical potential for data-analysis and find as many as seven parameters independent of incident energy. The parameters $R_0 = 9.9$ fm, $B_0 = 42.6$ MeV, $B_1 = 3.0$, $B_2 = 0.15$, $R_{0W} = 10.5$ fm, $W_0 = 8.2$ MeV, and $W_1 = 0.6$ are found energy-independent when we explain the experimental findings by using the potential. Other three parameters placed in the table 1 vary with the incident energies.

We compare theoretically calculated angular elastic scattering cross sections with the experimental values in the given range of incident energies. All l-values, i.e. $l = 0$ to $l_{\rm max}$, ($l_{\rm max} = 40$ for this system), are considered for determining theoretical scattering cross sections. The higher order angular momentum components have not been neglected. All the experimental data are extracted from site http://nrv.jinr.ru. with respect to the [24, 25].

All the plots in figure 4 for different incident energies show comparison of theoretical calculations with corresponding experimental results. Comparison of calculated values with the experimental outcomes promises quite a good explanation of the cross sections.

We compare the fifth panel of figure 4 with figure 5; both the plots are given for the same incident energy, i.e. $E_{\rm c.m.} = 15.84$ MeV. We try to explain the experimental results without invoking the *analytic-junction feature* in figure 5, but fail to match the data points. The theoretical result with $R_0 = 0$ is shown in figure 5 by a solid curve (blue), which deviates from the experimental values represented by circles (red). Here, the condition $R_0 = 0$ results in the absence of outer region. Similarly, $R_{0W} = 0$ imposes the condition for the absence of inner region, with which the theoretical result is shown by a horizontal straight segment that largely deviates from the experimental data. Thus, our theoretical calculations agree to the experimental data if both the regions are considered simultaneously. Hence the essentiality of the feature in our potential is understood.

3.2. Variation of reflection function $|S_l|$

The fact that the behaviour of S-matrix is imperative for elastic scattering is understood from equation (12). The reflection function $|S_l|$ and its counterpart $|1–S_l|$ for the elastic system ^{6}Li + ^{90}Zr are shown in figure 6 for different 'l' values ranging from $l = 0$ to $l = 40$ at the incident energy, $E_{\rm c.m.} = 31.87$ MeV. Initial horizontal portion of curve $|S_l|$ indicates that low partial waves are absorbed to a greater extent and contribute towards nuclear reactions while the partial waves for $l > 13$ are effective in the Coulombic region. The absorptive domain is clearly distinguished from pure Coulombic domain (upper horizontal portion) where $|S_l|$ value becomes a perfect unity for $l > 36$. Thus we have a large transition region, having quite large span, $\Delta l = 23$. In fact, large value of Δl permits the dominance of more number of partial waves in the transition region. This results in a smooth behaviour in $\sigma_{\rm el}/\sigma_{\rm Ruth}$ as proposed by Agarwalla *et al* [27]. When the value of V_{BW} in our potential is kept low at the surface region, this allows a significant number of partial waves to enter the interior region of the potential. Barrier waves are scattered from barrier and internal waves enter the interior region. Superposition of barrier waves with internal waves via the analytic-junction feature in the effective potential gives desired scattering results.

Table 1. Values of energy-dependent parameters for the system ^{6}Li + ^{90}Zr.

$E_{c.m.}$ (MeV)	V_B (MeV)	V_{BW} (MeV)	W_2
10.19	1.5	0.9	0.2
11.11	1.6	1.0	0.6
12.07	1.48	1.1	0.25
13.95	1.3	1.2	0.2
15.84	0.9	1.9	0.12
17.71	0.8	1.7	0.09
19.60	1.1	1.0	0.05
23.36	1.15	1.1	0.07
28.05	1.15	1.0	0.1
31.87	1.15	1.0	0.13

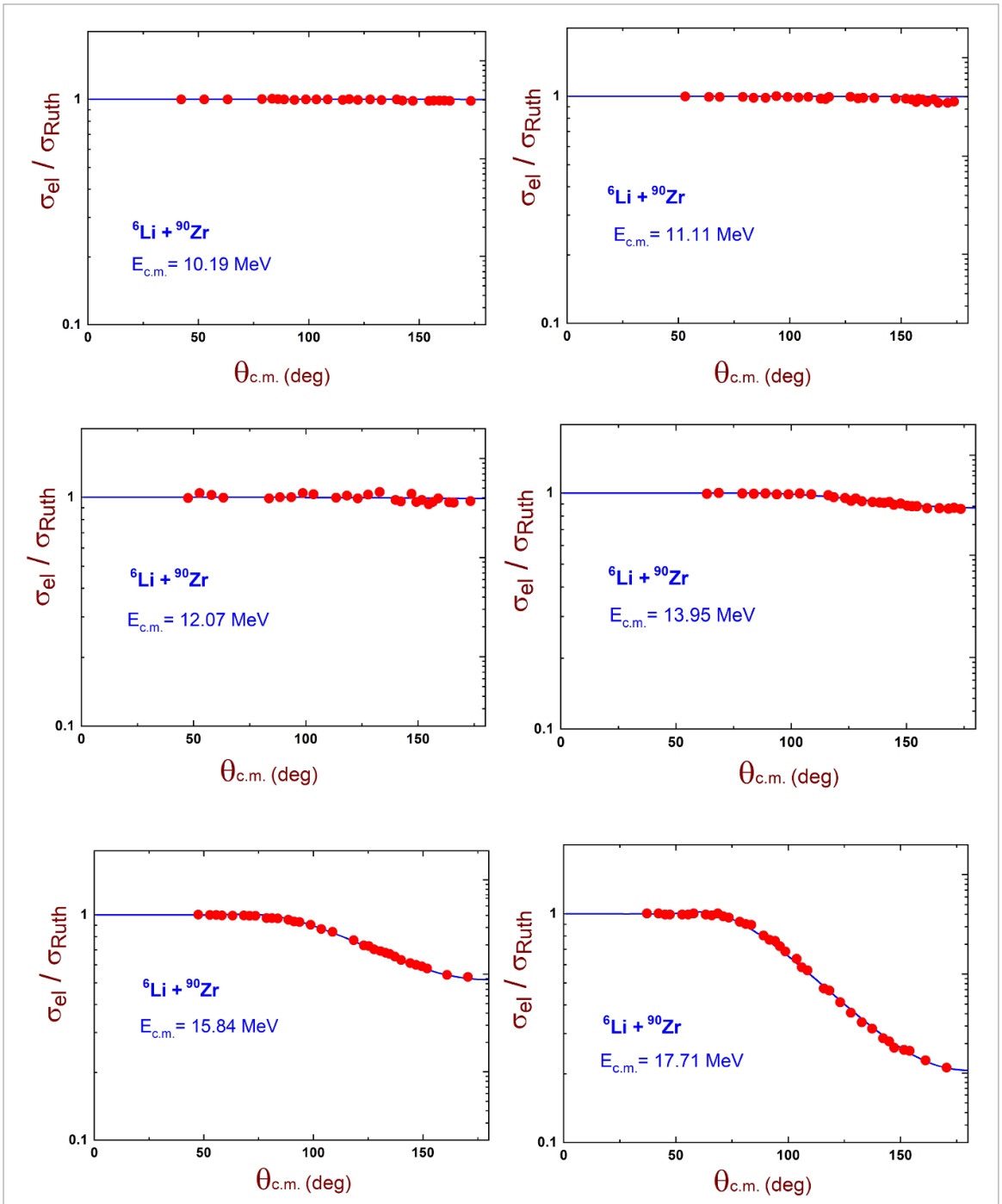

Figure 4. Angular variation of scattering cross-sections of the elastic collision system ^{6}Li + ^{90}Zr at different incident energies, namely, 10.19, 11.11, 12.07, 13.95, 15.84, 17.71, 19.60, 23.36, 28.05 and 31.87 MeV in c.m.-frame. Theoretical values are represented by solid curves (blue), whereas, the experimental values taken from http://nrv.jinr.ru. for [24, 25]. are represented by circles (filled with red color).

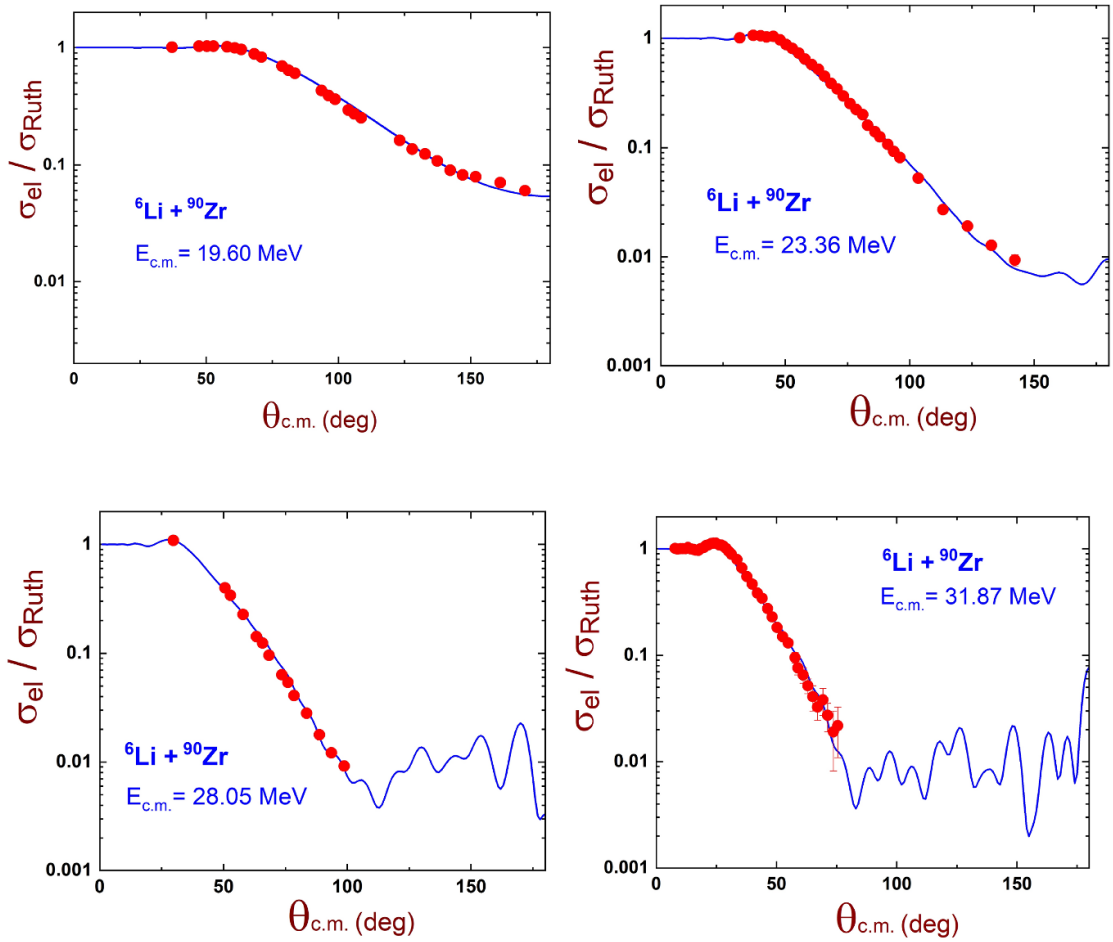

Figure 4. (Continued.)

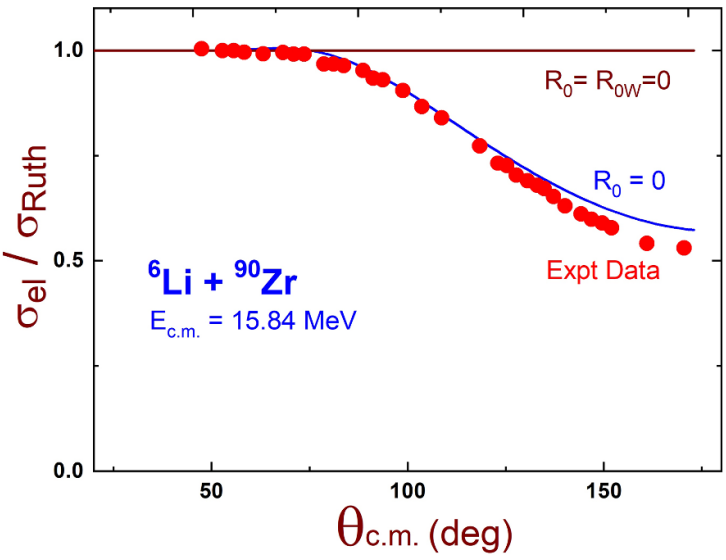

Figure 5. Comparison of theoretically calculated angular elastic scattering cross-sections with experimentally measured values at $E_{c.m.} = 15.84$ MeV for $R_0 = 0$ and $R_0 = R_{0w} = 0$ without taking analytic-junction feature into consideration.

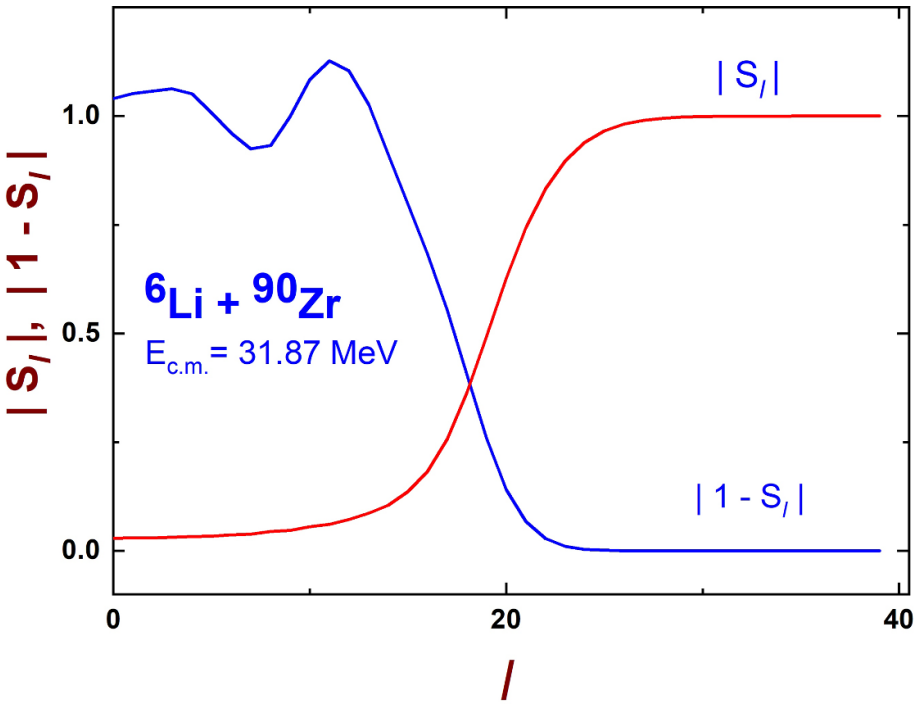

Figure 6. Plot of $|S_l|$ and $|1–S_l|$ versus l for ^{6}Li + ^{90}Zr at $E_{c.m.} = 31.87$ MeV with parameters mentioned.

Certain aspects of the experimental data may not be described by the standard optical model. Therefore, extra terms are added to the standard nuclear potential to modify its monotonic variation with radial distance. Such modification helps explain the experimental results. Total real potential of Boztosun [28] consists of the nuclear potential with two small additional potentials $U_1(r)$ and $U_2(r)$. Similar modifications in optical potential by Mackintosh [29], Kobos [30, 31], and Ordonez [32] have explained certain complicated aspects of the experimental data. We do not add similar additional terms to our potential, but the inbuilt analytic-junction structure serves our purpose in heavy ion elastic collision systems.

3.3. Notch test and radial sensitivity

No doubt, the optical model potential is widely accepted for studying nuclear reaction mechanism [33], but there can be a number of possible families of parameters, as suggested by *Igo ambiguity* [34], to explain the same elastic experiment. It is apt to discuss the optical model within sensitive region [35] in order to determine the parameters accurately. The *notch perturbation method* is one of few successful methods to get the radial region of potential sensitivity.

The sensitivity of optical model analysis can be tested by using a localized perturbation of the radial nuclear optical potential. Accordingly, a notch test analysis of our potential is done to check its radial sensitivity. The perturbation cuts a notch out of the potential. Our main aim is to examine the effect of perturbation in the cross section as the position of the perturbation is varied systematically. The authors have successfully tested the radial sensitivity of the present nuclear potential for the system ^{58}Ni + ^{27}Al [36].

The perturbed potential is given as

$$V_{\text{pert}} = V_{\text{n}}(r,R,b) \; - \; V_{\text{n}}(r,R,b).f_{\text{notch}}(r,R',b') \tag{13}$$

$$\text{where } f_{\text{notch}}(r,R',b') = \frac{1+\tanh(r-R')b'}{\cosh^2(r-R')b'}.$$

This is obtained by considering the radial part of our potential described in equation (2). The position and shape of notch are determined by R' and b'. The parameter b′ is given as $b' = \frac{\sqrt{2\mu V'}}{\hbar^2 B'}$. The perturbation for the system is shown in figure 7 at $E_{c.m.} = 17.71$ MeV. The dashed line shows unperturbed potential, whereas, the solid curve gives perturbed potential with a notch at $R' = 5$ fm for $V' = 15$ MeV and $B' = 0.1$. By changing the value of B' from 0.1 to 03 and 0.5, we get two extra notches at the same position. The mouth of the notches becomes wider with increase of B' value, but the positions remain the same. The calculated elastic angular distribution changes greatly at the notch.

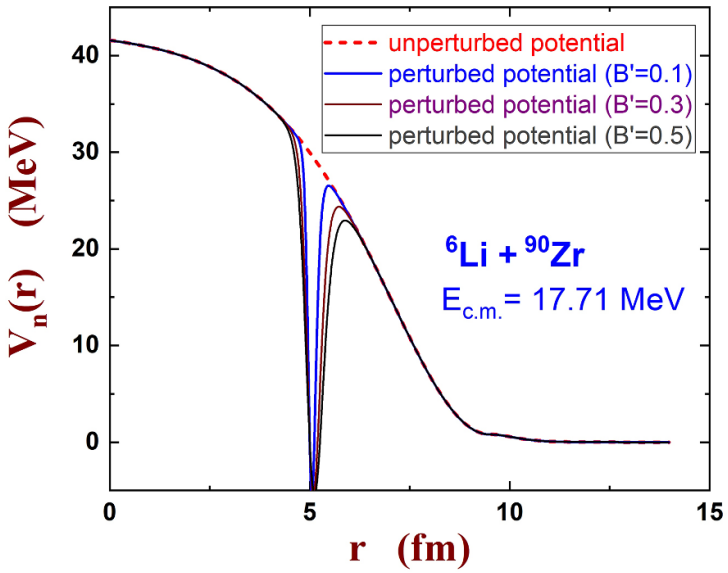

Figure 7. Comparison of unperturbed potential with perturbed potential for the system ^{6}Li + ^{90}Zr at $E_{c.m.} = 17.71$ MeV. The dashed curve shows the unperturbed potential and the solid curve shows the perturbed potential with a notch at $R' = 5$ fm for $V' = 15$ MeV. Three notches are found at the same position for three values of B', i.e. $B' = 0.1$, 0.3 and 0.5. The dashed curve is clearly seen only at the notch region, but present above and below the notch region.

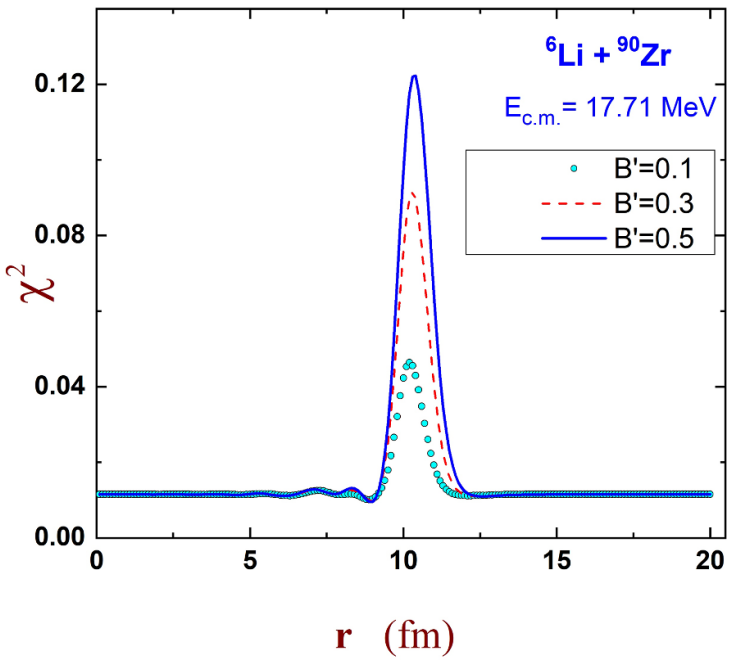

Figure 8. Plot of χ^2 to show the radial sensitivity of the optical model potential used for analysis of the elastic system ^{6}Li + ^{90}Zr at $E_{c.m.} = 17.71$ MeV. Three peaks of different heights are obtained at the same position for three values of B', i.e. $B' = 0.1$, 0.3 and 0.5.

The radial sensitivity is inferred well from figure 8, where the χ^2 (chi-square) analysis is given by changing the position of the notch along r with $B' = 0.1$, 0.3 and 0.5. The main peak of the real part is due to direct scattering process. The cause of tiny peak may be due to far-side interference effect. The potential at the centre ($r = 0$) of the nucleus is difficult to determine. However the behaviour of potential at the centre is irrelevant for us as we are interested in elastic scattering.

3.4. Variation of real and imaginary parts with incident energy

When we explain experimental scattering data with the best fit at different incident energies, we find the real and imaginary parts of the potential nearly energy-independent at higher values of energies. But their variation is phenomenal near the Coulomb barrier.

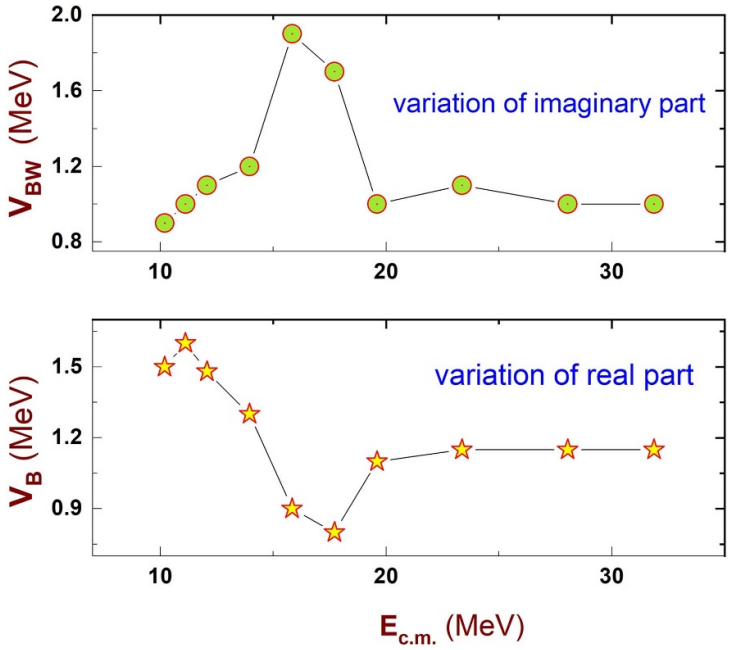

Figure 9. Variation of real part V_B and imaginary part V_{BW} of the optical potential obtained with the best fit for the elastic scattering system $^{6}Li + {}^{90}Zr$. The Coulomb barrier is taken as 16.9 MeV in the c.m.-frame.

The variations in the real part and imaginary part with the change of incident energy may be explained through dispersion relations [5, 37], which are built from the principle of causality. The real and imaginary parts of the optical potential used in [24]. are connected through a dispersion relation given by

$$V(r,E) = V_0(r,E_s) + \frac{P}{\pi}(E-E_s) \times \int_0^{\infty} \frac{W(r,\,E')}{(E'-E_s)(E'-E)} \mathrm{d}E' \tag{14}$$

where V and W are the real and imaginary parts of the optical potential. The second term is attractive polarization potential. The imaginary potential W has little effect in the second term at low energy; therefore V_0 is normalized at energy E_S.

The real part V_B of our potential, as depicted in the bottom-layer of figure 9, remains nearly constant around 1.15 MeV at high energies, but falls near the Coulomb barrier and undergoes a small change of 0.35 MeV. In case of imaginary part V_{BW}, as depicted in the top-layer of figure 9, the potential remains almost constant around 1.0 MeV at higher values of incident energy, but it sharply increases to a value of 1.9 MeV as the magnitude of incident energy approaches the neighbourhood of Coulomb barrier, and then it decreases. Thus, we observe an increase of the imaginary potential as the energy decreases, whereas, the real part undergoes a small reduction near the barrier. Such variations in the real and imaginary parts of the optical potential follows the trends of variation of real and imaginary parts of [24]. in which such variations correspond to the presence of 'breakup threshold anomaly' (BTA), the phenomenon we expect when one of the colliding partners is weakly bound nucleus.

3.5. Comparison of reaction cross sections

An optical model (OM) analysis of the experimental values of elastic scattering differential cross section was performed in [24] using FRESCO code. Further the data were analyzed in the continuum-discretized coupled-channel (CDCC) approach. Our theoretical values of the reaction cross sections (σ_R) at various energies are given in table 2 along with the cross-sections obtained from the two approaches of [24]. in the same range.

The reaction cross sections obtained from three different approaches are compared in figure 10. The reaction cross sections obtained by the OM (FRESCO) approach and CDCC approach are represented by circles and stars respectively. The corresponding reaction cross sections obtained by our theoretical calculation are represented by triangles. The figure shows the almost agreement of reaction cross sections from three different methods with minimal differences.

The magnitudes of reaction cross section at $E_{c.m.} = 31.87$ MeV are missing in column-2 and 3. It is because the value is not found in optical model approach using FRESCO code or CDCC approach. The value

Table 2. Reaction cross sections (σ_R) in millibarn (mb) at various energies for the system ^{6}Li + ^{90}Zr.

1	2	3	4	5
$E_{c.m.}$ (MeV)	OM	CDCC	Theo. calc.	Relative deviation
10.19	0.34	0.39	0.12	0.69
11.11	3.6	3.5	2.25	0.35
12.07	20.5	8.3	7.6	0.08
13.95	41.6	47.0	41.7	0.11
15.84	175.3	170.7	186.9	0.09
17.71	404.7	416.7	444.5	0.06
19.60	647.5	664.8	678.4	0.02
23.36	1085.8	1062.1	1153.1	0.08
28.05	1508.9	1398.2	1561.0	0.11
31.87	—	—	1822	—

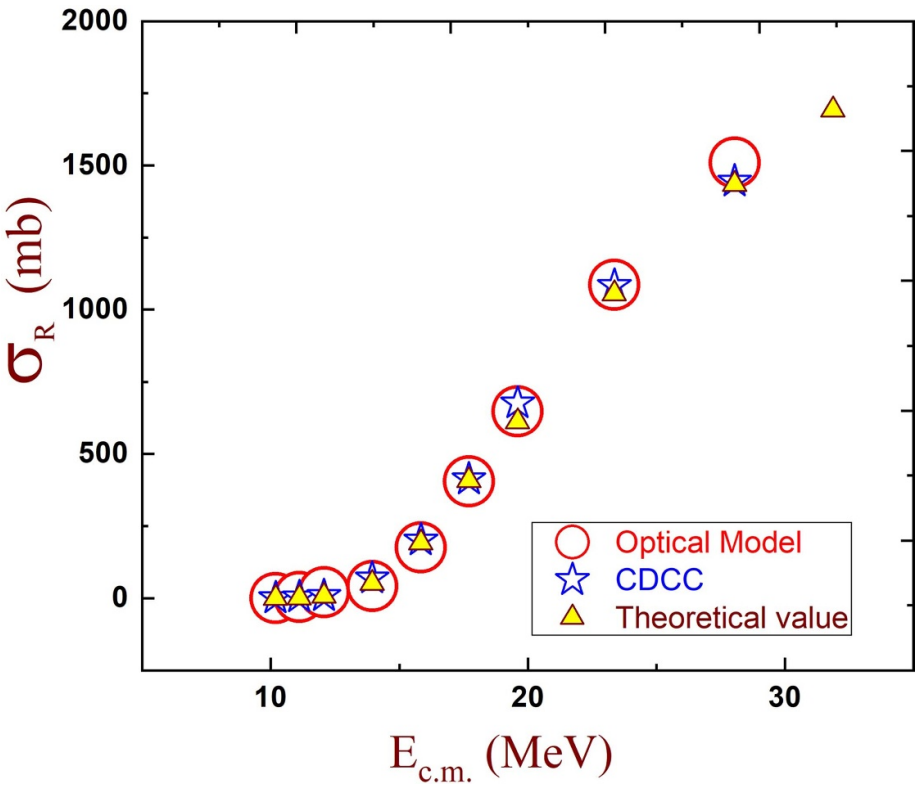

Figure 10. Plot of scattering reaction cross section at various projectile energies for the heavy ion collision ^{6}Li + ^{90}Zr. The reaction cross sections obtained by the optical model (OM) [21], the CDCC approach [21] and our theoretical calculation are represented by circles, stars, and triangles respectively.

$\sigma_R = 1822$ mb given under Column-4 for $E_{c.m.} = 31$ MeV is theoretically calculated by using our model. Column-5 of the table 2 shows that the relative deviations of theoretically calculated cross sections with respect to the values tabulated under column-3 obtained through CDCC approach using the formula:

$$\text{Relative deviation} = \frac{\text{CDCCvalue} \sim \text{Theor.value}}{\text{CDCCvalue}}.$$

4. Conclusion

The used optical potential with less number of energy dependent parameters successfully analyses angular distribution of elastic scattering cross sections of the system ^{6}Li + ^{90}Zr. The experimental values of the cross-sections for this system are almost reproduced by the potential. The behaviour of potential near the Coulomb barrier indicates the presence of breakup phenomena (BTA), which is usually expected in light-heavy interaction. The scatterings of heavier targets with lighter projectiles lead to breakup phenomena which may affect the nuclear potential in a different manner than the traditional heavy-heavy scattering. The

potential is capable of analyzing systems with heavy projectiles like ^{14}N, ^{19}F, ^{58}Ni in addition to collision systems with light projectiles like ^{6}Li. Thus the potential proves its versatility in explaining the experimental scattering results for the heavy as well as light projectiles. The study of collision of light projectile ^{6}Li with heavy target ^{90}Zr suggests that such phenomenon is dominated by nuclear breakup for which the imaginary part rises near the Coulomb barrier.

Our study is mainly based on Optical Model parameterization that enables us to evaluate nuclear cross-sections that are used in providing nuclear data for application purposes. The importance of these studies is made even more apparent by the worldwide diminution of experimental facilities for low energy nuclear physics measurements. The experimental scattering data for the system $^{6}\mathrm{Li} + {}^{90}\mathrm{Zr}$ is available for small range of incident energy $E_{\mathrm{c.m.}}$, i.e. 10.19 MeV to 31.87 MeV. Further, the cross-section data are missing when energy increases for higher angles, i.e. above 100°. Our study, especially for $E_{\mathrm{c.m}} = 23.36$, 28.05 and 31.87 MeV, will go a long way towards encouraging the experimentalists in order to perform experiments for wider energy range with wider angles and explore the system to a greater extent.

A study on dependence of reflection function $|S_l|$ on 'l' values agrees to the fact that the partial waves which contribute significantly to the elastic scattering have low l-values. Further the dependence of reaction cross section on the incident energy is studied and reaction cross section at $E_{\mathrm{c.m.}} = 31.87$ MeV is theoretically calculated using our formalism (figure 10). Angular distributions measured in a wide angular range extract the behavior of the potential reliably.

The successful analysis of various scattering systems may give an idea to a general reader about the shape of nuclear potentials and the changes of nuclear potentials with the change of the scattering properties. Further, this calculation can be used to study the fusion phenomena in sub-barrier region to see the structure phenomena which deserves the experimental verification.

Data availability statement

The data that support the findings of this study are available upon reasonable request from the authors.

Acknowledgments

Authors are thankful to Jajati Keshari Nayak (VECC, Kolkata) for helpful discussion and critical reading of the manuscript.

ORCID iD

Bidhubhusan Sahu https://orcid.org/0000-0003-3250-4628

References

[1] Satchler G R 1991 *Phys. Rep.* **199** 147
[2] Santra S, Singh P, Kailas S, Chatterjee A, Shrivastava A and Mahata K 2001 *Phys. Rev.* C **64** 024602
[3] Jena K K and Agarwalla S K 2021 *Proc. DAE Symp. Nucl. Phys.* vol **65** p 329
[4] Jena K K, Senapati S, Raj Preethi P, Prema P and Agarwalla S K 2021 *Proc. DAE Symp. Nucl. Phys.* vol **65** p 437
[5] Mahaux C, Ngô H and Satchler G R 1986 *Nucl. Phys.* A **449** 354
[6] Ferrero J L, Pacheco J C, Baeza A, Barrigon J M, Bilwes B, Bilwes R and Mau N V 1990 *Nucl. Phys.* A **514** 367–80
[7] Diaz J, Ferrero J L, Ruiz J A, Bilwes B and Bilwes R 1989 *Nucl. Phys.* A **494** 311
[8] Fulton B R, Banes D W, Lilley J S, Nagarajan M A and Thompson I J 1985 *Phys. Lett.* B **162** 55
[9] GuiQing H U *et al* 2000 *Chin. Phys.* C **24** 725–31
[10] Chengjian L, Jincheng X Huanqiao Z Zuhua L Feng Y and Lixin L 1997 *Chin. Phys.* C **21** 872–80
[11] Figueira J M *et al* 2010 *Phys. Rev.* C **81** 024613
[12] Maciel A M M *et al* 1999 *Phys. Rev.* C **59** 2103
[13] Signorini C *et al* 2000 *Phys. Rev.* C **61** 061603(R)
[14] Gomes P R S *et al* 2005 *Phys. Rev.* C **71** 034608
[15] Deshmukh N N *et al* 2011 *Phys. Rev.* C **83** 024607
[16] Kumawat H *et al* 2020 *Nucl. Phys.* A **1002** 121973
[17] Gollan F *et al* 1984 *Nucl. Phys.* A **979** 87–101
[18] Hodgson P E 1971 *Rep. Prog. Phys.* **34** 765
[19] Mallick G S, Agarwalla S K, Sahu B and Shastry C S 2006 *Phys. Rev.* C **73** 054606
[20] Sahu B, Mallick G S and Agarwalla S K 2003 *Nucl. Phys.* A **727** 299–318
[21] Ginocchio J N 1984 *Ann. Phys., NY* **152** 203
[22] Jena K K, Senapati S, Sahu B B, Nayak J K and Agarwalla S K arXiv:2201.03805
[23] Jena K K, Agarwalla S K and Sahu B 2022 *Acta Phys. Pol.* B **53** 10–A1
[24] Kumawat H *et al* 2008 *Phys. Rev.* C **78** 044617
[25] Puigh R J and Kemper K W 1979 *Nucl. Phys.* A **313** 363–75
[26] Sahu B, Agarwalla S K and Shastry C S 2002 *J. Phys. A: Math. Gen.* **35** 4349
[27] Agarwalla S K, Mallick G S, Prema P, Mahadevan S, Sahu B and Shastry C S 2005 *J. Phys.* G **32** 165

[28] Boztosun I 2002 *Phys. Rev.* C **66** 024610
[29] Mackintosh R S and Kobos A M 1982 *Phys. Rev.* C **26** 1766
[30] Kobos A M, Satchler G R and Mackintosh R S 1983 *Nucl. Phys.* A **395** 248
[31] Kobos A M and Satchler G R 1984 *Nucl. Phys.* A **427** 589
[32] Ordonez C E and Cosman R J 1986 *Phys. Lett.* B **173** 39
[33] Brandan M E and Satchler G R 1997 *Phys. Rep.* **285** 143
[34] Igo G 1958 *Phys. Rev. Lett.* **1** 72
[35] Cramer J G and DeVries R M 1980 *Phys. Rev.* C **22** 91
[36] Jena K K, Sahu B B and Agarwalla S K 2022 *Proc. DAE Symp. Nucl. Phys.* vol **66** p 662
[37] Byron F W and Fuller R W 1992 *Mathematics of Classical and Quantum Physics* (New York: Dover) p 340